A novel NH_2-MIL-88B(Fe)-modified ceramic membrane for the integration of electro-Fenton and filtration processes: A case study on naproxen degradation

Zhihong Ye [1,2,3], Roger Oriol[2], Chao Yang[1], Ignasi Sirés[2,**], Xiao-Yan Li[1,*]

[1] *Environmental Engineering Research Centre, Department of Civil Engineering, The University of Hong Kong, Pokfulam, Hong Kong, China*

[2] *Laboratori d'Electroquímica dels Materials i del Medi Ambient, Departament de Química Física, Facultat de Química, Universitat de Barcelona, Martí i Franquès 1-11, 08028 Barcelona, Spain*

[3] *Key Laboratory of Eco-environments in Three Gorges Reservoir Region, Ministry of Education, College of Environment and Ecology, Chongqing University, Chongqing, China*

Paper submitted for publication in *Chemical Engineering Journal*

* Corresponding author: xlia@hku.hk (X.-Y. Li)

** Corresponding author: i.sires@ub.edu (I. Sirés)

Abstract

Process intensification based on innovative coupling between membrane microfiltration and catalytic oxidation technologies has become a promising strategy for water treatment. Here, a surface-nucleated metal-organic framework (MOF) was grown in situ to obtain an NH_2-MIL-88B(Fe)-functionalized catalytic ceramic membrane (NH_2-MIL-88B(Fe)@CM), whose ability to remove naproxen from water matrices via the so-called electro-Fenton with catalytic ceramic membrane (EFCCM) process was systematically investigated. The physicochemical properties of the NH_2-MIL-88B(Fe) and membranes were characterized by XRD, FTIR, XPS and SEM, revealing the formation of a well-defined NH_2-MIL-88B(Fe) layer on the porous CM with a thickness of around 13.5 μm, which provides a large amount of active sites for H_2O_2 activation to generate hydroxyl radical (•OH). The EFCCM treatment of naproxen in Na_2SO_4 solution under recirculation batch mode yielded almost complete drug removal in 90 min at 50 mA, and the stability and catalyst loss tests gave evidence of good membrane reusability for 5 cycles. The treatment of naproxen in urban wastewater confronted severe membrane fouling, but this was effectively mitigated by combining hot water backwash with EF self-cleaning. Finally, the naproxen degradation routes involving 7 byproducts are proposed. This is an effective approach to the fabrication of CCM, which could be used for wastewater treatment in continuous mode as suggested by the minimal NPX content at the membrane outlet.

Keywords: Electro-Fenton; Membrane filtration; Metal-organic framework; Pharmaceutical; Water decontamination

1. Introduction

The electro-Fenton (EF) process, one of the most effective methods for electrochemical advanced oxidation, has gained a great attention in recent years, since it allows the complete destruction of refractory organic pollutants in a short timescale as a result of the massive formation of powerful hydroxyl radicals (•OH) via Fenton's reaction (1) [1-3]. In EF, the in-situ generation of H_2O_2 at a carbonaceous cathode through the two-electron oxygen reduction reaction (2) is highly efficient, which minimizes the inconveniences and costs associated to industrial H_2O_2. The simultaneous production of Cl_2 and adsorbed •OH from anodic Cl^- and water oxidation accelerates the destruction of pollutants and byproducts [4-8].

$$Fe^{2+} + H_2O_2 \rightarrow Fe^{3+} + {}^{\bullet}OH + OH^- \quad (1)$$

$$O_2(g) + 2\,H^+ + 2\,e^- \rightarrow H_2O_2 \quad (2)$$

Nonetheless, crucial concerns on the implementation of conventional EF arise from the catalyst source. Fenton's reaction with soluble Fe^{2+} demands strong acidic conditions (pH ~3.0) to achieve optimum performance, inevitably requiring subsequent neutralization and iron sludge disposal [9-11]. Alternatively, the use of solid catalysts gives rise to the so-called heterogeneous electro-Fenton (HEF) process, which extends the operation pH range to alkaline media and reduces the iron sludge production, although poor catalyst recycling may be an issue with conventional iron-rich solids [12-14]. In these systems, •OH is predominantly produced via reaction (3), which implies the decomposition of H_2O_2 by intrinsic or regenerated Fe(II) surface active sites [15,16]. The Fe(III)-to-Fe(II) conversion becomes the rate-determining step but, since it is too slow in many materials, negatively affecting the performance of the HEF process.

In practice, additional drawbacks of conventional solid catalysts include their limited number of exposed active sites and an inefficient contact with relevant species like H_2O_2 or organics [16].

$$Fe(II) + H_2O_2 \rightarrow Fe(III) + {}^{\bullet}OH + OH^{-} \quad (3)$$

Recently, iron-based metal-organic frameworks (Fe-MOFs) with high porosity and large surface area, uniform and abundant distribution of iron sites, controllable morphology and good Fe(III)-to-Fe(II) conversion have been investigated as superior catalysts in Fenton-based advanced oxidation processes [17-19]. Among them, MIL-type (Materials Institute Lavoisier) structures like MIL-53(Fe), MIL-100(Fe), MIL-101(Fe), MIL-88A(Fe) and MIL-88B(Fe) exhibited excellent catalytic performance in Fenton's reaction [20]. MIL-88B(Fe), synthesized from trimeric iron clusters and 1,4-benzenedicarboxylic acid (H_2BDC) ligands, seems advantageous due to its abundant, accessible and unsaturated open iron sites [21]. H_2O_2 can be easily adsorbed onto such sites by replacing the non-bridging ligands and, concomitantly, the electron donation from electron-rich H_2BDC ligands to Fe(III) centers favors the Fe(II) regeneration that sustains reaction (3) [22]. Gao and co-workers demonstrated the superiority of MIL-88B(Fe) over iron oxides and MIL-53(Fe) or MIL-100(Fe) for phenol removal by HEF process [23]. Likewise, further studies demonstrated that the presence of electrophilic groups in the organic ligands reduces the electron density of the Fe(III) centers, thereby facilitating their reduction to Fe(II) [24]. For example, the introduction of electron-rich -NH_2 groups into MIL-88B(Fe) upon substitution of H_2BDC by NH_2-BDC ligands yields NH_2-MIL-88B(Fe). In some cases, the enhanced electron transfer efficiency may be accompanied by the easier capture of pollutant molecules due to the presence of hydrophilic amino groups [25].

Despite the good performance of NH_2-MIL-88B(Fe) in HEF process, this catalyst has always been employed in its suspended form. In this scenario, particle aggregation reduces the $^{\bullet}OH$ productivity; moreover, the separation post-treatment required at the end is expensive and slow and, actually, it may become ineffective to recover small particles. The presence of catalyst residues in the treated solution is detrimental for water quality [26]. In response to these issues typically encountered for all heterogeneous catalysts, different substrates have been employed to support them [27]. The development of catalytic reactive membranes is particularly appealing, owing to the process intensification that potentially derives from the integration of filtration and degradation, which goes beyond the more classical 2-step technology [28]. Standard micro/ultra/nanofiltration and reverse osmosis membranes display numerous advantages in large-scale wastewater treatment, although some challenges related to membrane fouling and low rejection efficiency towards small organic molecules still remain [29]. Surface catalysis at filtration membranes has thus great potential to solve deficiencies like deactivation of suspended catalysts and fouling of unmodified membranes [30]. Furthermore, the filtration process is expected to improve the mass transport of organic molecules towards the coated catalyst, thus accelerating the oxidation events [31].

Recently, low-pressure membranes, commonly operated at transmembrane pressure (TMP) < 2 bar, have gained attention due to the high-quality produced water, minimized cost and small footprint [32,33]. Among them, ceramic membranes (CM) are superior to polymeric counterparts thanks to their greater mechanical, chemical and thermal stability, higher corrosion resistance, extended duration and higher filtration flux [34]. Hence, the development

of catalytic ceramic membranes (CCM) to integrate microfiltration with robust oxidation technologies becomes a promising strategy. For instance, Plakas el al. fabricated a novel Fe_3O_4 nanoparticles-coated CM for heterogeneous Fenton-like oxidation of micropollutants in drinking water [27]. Liu et al. explored the photo-Fenton activation, filtration and antifouling performance of FeOCl-coated CM [26], whereas Wu et al. developed an MnO_2-loaded CM for peroxymonosulfate activation, attaining an excellent degradation of 4-hydroxylbenzoic acid [35]. Nevertheless, as far as we know, the design of MOFs-based CCM to be integrated in the HEF treatment of low molecular weight micropollutants has not been addressed so far.

Herein, an NH_2-MIL-88B(Fe)-coated ceramic membrane (NH_2-MIL-88B(Fe)@CM) has been developed for the first time to integrate microfiltration and HEF methods in the so-called EF with catalytic ceramic membrane (EFCCM) process for the removal of naproxen (NPX) from water. NPX is a common non-steroidal anti-inflammatory drug for fever relieving and inflammation reduction [36,37,38], being frequently detected in municipal wastewater plants and surface water. NPX was spiked into model matrices and urban wastewater at natural pH, thereby being treated by NH_2-MIL-88B(Fe)@CM-enhanced EF process in an IrO_2/air-diffusion cell. The CCM was prepared via in-situ growth of NH_2-MIL-88B(Fe) and its physicochemical properties were analyzed in detail. The influence of initial pH, flow rate and applied current on the NPX removal by the EFCCM process has been thoroughly investigated, whereas the byproducts generated were determined by gas chromatography coupled to mass spectrometry (GC-MS). The recyclability, stability and antifouling characteristics of NH_2-MIL-88B(Fe)@CM have been assessed to ensure a good degree of cleaning and recovery.

2. Experimental

2.1. Chemicals

Naproxen sodium (98% purity) was purchased from Sigma-Aldrich. Sodium sulfate, chloride, bicarbonate and hydroxide pellets as well as sulfuric acid (96%-98% purity) were of analytical grade from Merck. $FeCl_3$•$6H_2O$ and 2-aminoterephthalic acid (NH_2-BDC) from Sigma-Aldrich and dimethylformamide (DMF) from T.C.I. were employed for the synthesis of the NH_2-MIL-88B(Fe). $TiOSO_4$ used for H_2O_2 determination, 1,10-phenantroline monohydrate and ascorbic acid employed to determine the dissolved iron concentration and 5,5-dimethyl-1-pyrroline-N-oxide (DMPO) needed for electron spin resonance (EPR) analysis were acquired from Sigma-Aldrich. All the other required chemicals were of analytical or high-performance liquid chromatography (HPLC) grade supplied by Merck and Sigma-Aldrich. All model and standard solutions were prepared with Milli-Q water (ρ > 18.2 MΩ cm). The main characteristics of the urban wastewater, collected from Stanley Sewage Treatment Works (Hong Kong), are described in Supplementary Material file (Text S1).

2.2. Preparation of the NH_2-MIL-88B(Fe)@CM

Commercial CM plates, made of α-Al_2O_3 and supplied by Sinotsing Environment Corporation (China), were employed for the preparation of the NH_2-MIL-88(Fe)@CM. The synthesis procedure is schematized in Fig. S1. The ceramic substrate was first immersed into 0.3 wt.% poly(sodium 4-styrenesulfonate) (PSS, MW ~10,000 g mol^{-1}) aqueous solution for 30 min at 60 °C, being subsequently rinsed with deionized water and dried in an oven at 80 °C. Afterwards, the PSS-grafted ceramic substrate was immersed into 40 mL of a methanol

solution, prepared with 1.5 mmol $FeCl_3$•$6H_2O$, for 30 min at 60 °C, followed by rinsing with methanol. After drying at 80 °C, the modified CM was immersed into a 35 mL of a DMF solutions containing 1.5 mmol $FeCl_3$•$6H_2O$ + 1.5 mmol NH_2-BDC. The content was then transferred to an autoclave for undergoing a solvothermal treatment for 4 h at 140 °C. To ensure a total coating of the CM with multiple layers, this process was repeated three times. After the last step, the NH_2-MIL-88B(Fe)@CM was washed with ethanol and water, repeatedly. Before use, the NH_2-MIL-88B(Fe)@CM was activated and cleaned with ethanol and water at flow rate of 1 mL min^{-1} for 30 min.

2.3. Catalyst characterization

The morphology of the NH_2-MIL-88B(Fe)@CM was observed by field-emission scanning electron microscopy (FESEM) using a Hitachi S-4800 microscope. It was coupled to an X-Max 80 detector, employed for elemental mapping by means of energy dispersive X-ray (EDX) analysis. The X-ray diffraction (XRD) analysis of the NH_2-MIL-88B(Fe) powder was made on an X-ray powder diffractometer (Bruker D8 Advance) using Cu $K_{\alpha 1}$ radiation operating at 40 kV and 20 mA. X-ray photoelectron spectroscopy (XPS) measurements for elemental analysis were performed in an ultrahigh vacuum spectrometer equipped with a VSW Class WA hemispherical electron analyzer, whereas high resolution XPS measurements for band alignment were performed on a Thermo Scientific K-Alpha spectrometer. The Fourier transform infrared (FTIR) spectra were collected using a PerkinElmer Spectrum One FTIR spectrometer (USA). The pore size distribution of pristine and coated membranes was analyzed by means of a PSDA-20 porometer (GaoQ Funct. Mater. Co., Ltd., China) using liquid–liquid

displacement porometry (LLDP) based on the capillary flow method. The hydrophilicity of membranes was estimated by measuring contact angles with a JC2000A contact angle goniometer (Shanghai Zhongchen Digital Technical Equipment Ltd., China).

2.4. Experimental setup and analytical procedures

All the experiments were carried out in a single-compartment glass cell with capacity of 180 mL of solution, at room temperature and under constant magnetic stirring. The experimental setup is illustrated in Fig. S2a, which is accompanied by a digital photograph shown in Fig. S2b. The anode (3 cm^2 of immersed area) was an IrO_2-based plate (1 mm of thickness) purchased from NMT Electrodes (South Africa), although in some trials a boron-doped diamond (BDD) thin film supported on a Si wafer (NeoCoat, Switzerland; 1 mm of thickness) was employed for comparison. The cathode was a 3 cm^2 commercial carbon cloth coated with carbon-PTFE (Sainergy, India), which served as a gas-diffusion electrode (GDE) once mounted as reported before [14]. The GDE was fed with air flowing from a pump at 1 L min^{-1} to ensure a continuous H_2O_2 generation. The anode-cathode distance was close to 1.0 cm to minimize the resistance. The membrane (28 mm × 34 mm), which was coated on both sides, was immersed into the solution to be treated and fixed. A peristaltic pump was used to filter the solution at a constant flow rate, while the membrane effluent was recycled back to the electrochemical cell. During membrane filtration, the TMP was continuously measured and recorded by a pressure transmitter and intelligent paperless recorder (SIN-P300 and SINR200D, Sinomeasure). Samples were withdrawn from the cell at sampling point 2 shown in Fig. S2a; otherwise, for selected trials the sampling was made at point 1 (Fig. S2a) and, in all cases, the samples were filtered with 0.2 μm

PTFE syringe filters. After each trial, backwashing with Mill-Q water at flow rate of 1 mL min^{-1} was performed for 30 min to restore the membrane properties.

The electrolytic trials were carried out at constant current provided by a DC power supply (IT6322A model from ITECH, China). The electrical conductance of the freshly collected wastewater was determined with a Metrohm 644 conductometer. The pH was measured with a Starter 3100 pH-meter (Ohaus, USA). The H_2O_2 concentration accumulated during the electrochemical assays was determined colorimetrically with an acidic Ti(IV) solution using a Shimadzu 1800 UV/Vis spectrophotometer (maximum absorbance at λ = 408 nm) thermostated at 25 °C. The concentration of total dissolved iron during the trials was obtained from the absorbance of the reddish complex formed once reacted with 1,10-phenanthroline, employing the same spectrophotometer (maximum absorbance at λ = 510 nm). Specifically, 4 mL of sample were mixed with 1 mL of 1 g L^{-1} 1,10-phenanthroline solution + 1 mL acetate buffer solution. The TOC content of the samples was analyzed immediately after collection, using a Shimadzu TOC-L analyzer.

The NPX concentration was determined on a Waters Acquity ultraperformance liquid chromatograph (UPLC). The separation was made with an Alltima C18 column (5 μm, 250 mm × 4.6 mm) at 30 °C, whose outlet was connected to a photodiode array (PDA) detector set at 231 nm. The mobile phase consisted in a mixture of acetonitrile and 10 mM KH_2PO_4 solution at pH 3.0 (50:50, v/v) that was eluted at 1.0 mL min^{-1}, yielding a NPX peak at 8.2 min.

The electron spin resonance (ESR) spectra were obtained with a Bruker ESP300E spectrometer at room temperature, using DMPO as $^{\bullet}OH$ trapping agent (Text S2). The organic

byproducts accumulated during the electrochemical treatment of NPX were identified by GC-MS analysis performed in a 6890 N chromatograph coupled to a 5975C mass spectrometer, both from Agilent Technologies, working in electron impact mode at 70 eV. A Teknokroma Sapiens-X5 ms and an HP INNOWax column (nonpolar and polar, respectively) with dimensions of 0.25 μm, 30 m × 0.25 mm were used. The organic components in the samples were recovered via liquid-liquid extraction with CH_2Cl_2 [39]. The mass spectra were identified from comparison with the NIST05 MS database.

3. Results and discussion

3.1. Characterization of the NH_2-MIL-88B(Fe)@CM

First, the as-prepared NH_2-MIL-88B(Fe) catalyst was characterized, as shown in Fig. 1. As can be observed in Fig. 1a, the XRD pattern displayed the main diffraction peaks at approximately 9.2˚ (002), 10.3˚ (101), 13.1˚ (102), 16.7˚ (103), 18.5˚ (200), 19.1˚ (201), 20.7˚ (202) and 29.5˚ (302), which are all consistent with the simulated pattern of the NH_2-MIL-88B(Fe) structure established from the crystallographic information file (CCDC No. 647646) [40]. It can thus be concluded that a pure NH_2-MIL-88B(Fe) catalyst was successfully synthesized. The chemical environment and electronic states of the elements contained in the NH_2-MIL-88B(Fe) powder were further investigated by XPS analysis, as shown in Fig S3 and 1b. The full spectrum (Fig. S3a) illustrates the presence of Fe, C, N and O in the catalyst. The high-resolution XPS spectrum of Fe 2*p* (Fig. 1b) can be deconvoluted into two main peaks and one satellite peak. Those at binding energies of 710.7 eV and 724.3 eV can be ascribed to Fe

$2p_{3/2}$ and Fe $2p_{1/2}$, respectively, whereas the one at 714.8 eV is assigned to a satellite signal. A comparison with results from the literature indicates that Fe(III) is the dominant iron species in the catalyst [40,41]. In the core-level spectrum of N 1*s* (Fig. S3b), the peak located at 398.4 eV can be ascribed to the coordination-free amino N-H bonds in -NH_2-BDC ligands, whereas the peak centered at 400.0 eV can be accounted for the protonated C-NH_3^+ group [42]. FTIR analysis was conducted to further investigate the functional groups present in NH_2-MIL-88B(Fe). As depicted in Fig. 1c, two adsorption peaks at 3460 cm^{-1} and 3337 cm^{-1} arise from symmetric and asymmetric stretching vibrations of -NH_2 groups [43]. The peaks at around 1581 cm^{-1} and 1382 cm^{-1} can be attributed to the typical O-C-O framework that is widely presented in NH_2-MIL-88B(Fe) [44]. Furthermore, the vibration band at 1256 cm^{-1} is related to the C-N stretching mode, which confirms the incorporation of the -NH_2 groups. The characteristic peak at 769 cm^{-1} can be associated to the C-H bending vibration of the organic linkers [45]. In addition, the peaks at 521 cm^{-1} and 439 cm^{-1} correspond to the Fe-O stretching mode due to the bonding of iron centers and organic ligands [44].

The surface and cross-section morphologies of the original and modified membranes were observed by FESEM (Fig. 2). The image of the pristine CM (Fig. 2a) displays a rough and porous surface structure with an approximate surface pore size of 2.0 µm. This value is close to the mean total pore size determined by porosimetry (2.41 µm, Table 1). From the surface SEM image of the NH_2-MIL-88B(Fe)@CM (Fig. 2b), typical spindle-shaped NH_2-MIL-88B(Fe) crystals were uniformly and tightly dispersed on the membrane without significant changes in their morphology [25,44]. The crystals were either attached to the membrane or stacked

together, thereby filling most of the surface pores and creating surface defects. The resulting higher complexity of the pore structure may result in a longer residence time of the organic molecules in the membrane, thus enhancing their contact with the adsorbed •OH. The cross-section SEM images of the NH_2-MIL-88B(Fe)@CM in Fig. 2c and 2d allow distinguishing a dense skin (i.e., outer layer) with thickness of about 13.5 μm attributed to the NH_2-MIL-88B(Fe) crystals immobilized on the CM. It is also evident that the crystals were partially intercalated in the internal channels (red arrows in Fig. 2d). The EDX mapping of the NH_2-MIL-88B(Fe)@CM cross-section image (Fig. 2e) confirms that the NH_2-MIL-88B(Fe) were predominantly distributed on the CM surface, whereas a smaller amount of Fe and N was identified inwards. Therefore, the proposed synthesis allowed the CM decoration even inside the pores, rather than a mere surface modification.

Table 1 summarizes the properties of the pristine and NH_2-MIL-88B(Fe)-decorated CM. The catalyst loading was approximately 100 mg. The pure water permeability using the NH_2-MIL-88B(Fe)@CM was much lower than that with the pristine membrane because of the dense and compact catalyst layers formed on the CM and the usage of PSS polymer during the synthesis. The compatibility of NH_2-MIL-88B(Fe) with the membrane and the stability are expected to be improved due to the coordination interactions between iron ions and the functional groups of the PSS chains [46]. Thus, the addition of PSS favors the increase of thickness of the catalyst layer, although at the same time it also increases the resistance to water transport. The mean pore size was reduced from 2.41 to 1.99 μm due to the dense stacks of NH_2-MIL-88B(Fe) particles on the CM surface. However, the decrease of porosity was less

significant (1.4%, Table 1), suggesting that the interstices between catalyst particles created additional porous structures. Moreover, the water contact angle was more than halved upon coating, in agreement with the increased hydrophilicity conferred by the amino groups in the NH_2-MIL-88B(Fe). This potentially endows the catalytic membrane with greater resistance to fouling [47].

3.2. Catalytic degradation of NPX solutions

Fig. 3a shows the NPX concentration decay during the treatment of 0.060 mM (10 mg C L^{-1}) NPX solutions with 0.050 M Na_2SO_4 at natural pH ~6.2 under different conditions. Prior to investigating the catalytic degradation performance, the NPX elimination by adsorption or membrane rejection was evaluated. As shown in Fig. S4, the rejection of NPX upon filtration with the pristine CM at 2 mL min^{-1} was around 30%. Beforehand, rejection of the small drug molecules as a result of size exclusion was expected to be negligible; in addition, electrostatic interactions could not be considered either due to the absence of functional groups in the CM [27]. Nonetheless, the relatively hydrophilic nature of NPX (log K_{ow} = 3.18) enabled its moderate encapsulation in the hydrophilic Al_2O_3 substrate, although such weak interaction could not ensure a stable adsorption/retention of NPX. Therefore, a remarkable fluctuation in the NPX concentration occurred over time, ending in a low final removal [48]. When the same treatment was made with the NH_2-MIL-88B(Fe)@CM at 2 mL min^{-1}, a relatively stable NPX removal was achieved (Fig. 3a), disappearing by 40% at 90 min. The NPX molecules are mainly ionized in a solution at pH ~6.2, owing to deprotonation ($pK_{a,NPX}$ = 4.15), whereas the NH_2-MIL-88B(Fe) particles tend to be positively charged at pH < 8.0 [48,49]. The

straightforward electrostatic interactions between NPX and NH_2-MIL-88B(Fe), along with the improved hydrophilicity of the membrane (discussed above from data in Table 1), favored the partial rejection of NPX. Regarding the electrochemical trials, Fig. 3a highlights a low NPX disappearance of 34% after 90 min of electro-oxidation (EO) treatment with an IrO_2-based anode combined with cathodic H_2O_2 production in the absence of the CCM, as expected from the mild degradation caused by IrO_2(•OH) generated from water oxidation [8]. Note that the contribution of H_2O_2 as oxidant, at a concentration of ~20 mM that is typical with similar setups [8], was null (not shown). The HEF process catalyzed by supported NH_2-MIL-88B(Fe) (with no solution pumping, aiming to discard the contribution of filtration) led to a substantial NPX concentration decay of 65% at 90 min, which corroborates the occurrence of heterogeneous Fenton's reaction (3) and the good catalytic activity of the NH_2-MIL-88B(Fe) particles. Finally, the EFCCM treatment with pumping at 2 mL min^{-1} was clearly superior to all the previous trials, obtaining the highest NPX abatement (i.e., 97% at 90 min). Note that the NPX concentration decays depicted in Fig 3a resulting from reactive phenomena that involved hydroxyl radicals (EO, HEF, EFCCM) agreed with constant reaction rates that agreed with a pseudo-first-order kinetics. As can be seen in Fig. 3b, the kinetic rate constant in the EFCCM process was approximately ~2.5-fold and ~7-fold greater than those determined in HEF and EO, respectively. In order to assess the feasibility of a continuous operation mode in EFCCM, the NPX concentration decay at the membrane outlet (sampling point 2 in Fig. S2a, instead of point 1 chosen for the aforementioned experiments) during the EFCCM trial of Fig. 3a was analyzed. Fig. 3c shows an almost constant NPX removal of ~90% over 90 min, suggesting that

the great outcome from the combined filtration-degradation takes advantage of the highly effective retention/rejection + catalytic oxidation. In addition, the used membrane was cleaned by backwashing with 180 mL of Milli-Q water at flow rate of 2 mL min^{-1} for 1 h. The residual concentration of NPX in the rinsing solution was 0.67 mg L^{-1}, which means that almost all the NPX molecules can be effectively degraded during the EFCCM treatment, rather than simply separated by the membrane. An additional EFCCM trial, not shown here, was carried out with only 1 mg L^{-1} NPX to demonstrate the ability to remove drug traces; the final NPX concentration was below the limit of quantification (LOQ = 0.2 mg L^{-1}).

3.3. EFCCM treatment of NPX solutions under different conditions

The effect of various experimental factors, including flow rate, solution pH, applied current and electrolyte composition, on the performance of the EFCCM process was investigated using the undivided IrO_2/air-diffusion cell.

Fig. 4a illustrates the drug removal as a function of the treatment time at different flow rates (Q). The corresponding permeate flux (J_P) can be calculated as follows:

$$J_P = \frac{V}{A\Delta t} = \frac{Q}{A} \quad (4)$$

where V is the permeate volume, A is the working membrane area (38 cm^2) and Δt is the filtration time.

Flow rates ranging from 1.0 to 6.0 mL min^{-1} were fixed by controlling the rotating speed of the peristaltic pump, giving rise to J_P values from 15.8 to 94.8 L h^{-1} m^{-2}. The enhancement of the degradation efficiency at higher flow rate is evidenced in Fig. 4a, being particularly more significant when the flow rate was increased from 1.0 to 2.0 mL min^{-1}. Within this range, the

theoretical filtration time required for the whole NPX solution volume (180 mL) is halved, which means that at 2 mL min^{-1} all the solution can be filtered and the NPX molecules can contact with the adsorbed •OH, thus accelerating the decontamination. In contrast, further increase from 2.0 to 6.0 mL min^{-1} led to an insignificant improvement of the global NPX removal at 90 min, which can be explained by the sharp shortening of the residence time of the NPX and H_2O_2 molecules in the confined membrane pores [50]. Fig. 4b shows the corresponding variations in TMP vs. time at each flow rate. The increase in J_P, associated to a greater flow rate, resulted in a higher TMP that stabilized at around 2.4 and 4.8 kPa operating at 1.0 and 2.0 mL min^{-1}, respectively. A less constant value, gradually rising from 8.2 to 11.9 kPa was measured at 4.0 mL min^{-1}. Such instability was more pronounced at 6.0 mL min^{-1}, with the TMP changing from 13.5 to 20.8 kPa within 90 min. The stable TMP at the lowest fluxes suggests the absence of membrane fouling thanks to the sufficient contact time that allowed the efficient degradation of NPX and its byproducts. Conversely, the more unstable TMP at high flux was deemed to compensate the membrane fouling caused by surface deposits and/or pore blockage with NPX and the intermediates due to their favored accumulation [31].

The influence of the initial solution pH on the drug disappearance during the EFCCM treatment was studied by varying this parameter between 3.0 and 9.0. As can be observed in Fig. 4c, the degradation rate was clearly enhanced as the pH became more acidic (note that pure adsorption trials performed at the same pH values, not shown here, yielded removals lower than 15%). The total removal was achieved after only 45 min at initial pH 3.0, which agrees with the optimum pH value for Fenton's reaction [24]. Despite this, it is remarkable that the overall

disappearance was also reached at initial pH 5.0 and 6.2 after 90 min, which is impossible in conventional homogeneous EF [1]. This demonstrates that the EFCCM process is advantageous to work over a wider pH range. The NPX removal decreased but was still high (74% at 90 min) at initial pH 9.0; this loss of performance can be ascribed to the lower oxidation potential of $^{\bullet}OH$ and the greater self-decomposition of H_2O_2 at alkaline pH [1,23]. The trends shown in Fig. 4c are also influenced by the potential occurrence of homogeneous Fenton's reaction (1). As shown in Fig. 4d, the solutions became more acidic in all cases, which is mainly explained by the production of organic products like carboxylic acids [44]. This favored the larger leaching and stabilization of iron ions in the solution (Fig. 4d). At pH ranging from 5.0 to 9.0, the dissolved iron content was very low (0.12-0.83 mg L^{-1}), suggesting the relatively high stability of the NH_2-MIL-88B(Fe) particles on the CM at mild pH. Therefore, in that pH range the heterogeneous Fenton's reaction (3) mainly accounted for NPX degradation. Conversely, at pH 3.0, the dissolved iron content was slightly greater, thereby allowing the contribution of homogeneous Fenton's reaction (1). This was beneficial for water decontamination, but negatively affected the membrane stability.

The positive effect of applied current can be deduced from Fig. 4e, especially when it was changed from 25 to 50 mA because it caused a significant enhancement in NPX removal, from 73% to 97%. This behavior can be attributed to the greater H_2O_2 accumulation (Fig. S5), which stimulated a higher $^{\bullet}OH$ production [39]. A larger $IrO_2(^{\bullet}OH)$ electrogeneration was also favored, although this presumably had a smaller relevance in the degradation process by EFCCM [51]. Current values greater than 50 mA did not led to such a substantial enhancement,

since the H_2O_2 surplus may accelerate the $^{\bullet}OH$ production from Fenton's reaction but it also consumes such radical in parasitic reactions.

The EFCCM performance in Na_2SO_4 medium under optimum conditions (Fig. 4a, 4c, 4e) was compared with that in $NaHCO_3$ and NaCl media (as these two are common salts in actual wastewater) with the same conductivity around 9-10 mS cm^{-1}, since this parameter determines the electrode potential in galvanostatic electrolysis. As shown in Fig. 4f, the presence of 0.009 M $NaHCO_3$ entailed a very poor NPX decay, only reaching 44% after 90 min. Indeed, HCO_3^- acts as an inhibitor because it scavenges the $^{\bullet}OH$, giving rise to much weaker radical like $CO_3^{\bullet-}$ [26]. In contrast, the addition of 0.035 M NaCl accelerated the NPX destruction, with overall abatement in only 45-60 min, which is ascribed to the participation of active chlorine as powerful oxidant.

The ability of the EFCCM process to remove not only NPX but also its reaction products was assessed by means of TOC analysis in 0.050 M Na_2SO_4 medium. Fig. S6 reveals a TOC abatement as low as 26% after 300 min using the IrO_2/air-diffusion cell at 100 mA, attributed to the formation of refractory molecules. Aiming to obtain a larger mineralization, the IrO_2 anode was replaced by BDD in order to produce a much stronger oxidant like BDD($^{\bullet}OH$). An excellent TOC removal (72%) was obtained, being the residual TOC related to persistent but non-toxic products like carboxylic acids (see comments on Fig. 4d).

3.4. Stability and reusability of the NH_2-MIL-88B(Fe)@CM

Despite the fact that NH_2-MIL-88B(Fe) has been proposed as an outstanding representative of stable MOFs in aqueous media, its decomposition during water treatment has been rarely

investigated. Herein, the stability of the NH_2-MIL-88B(Fe)@CM in water was evaluated from the time course of dissolved iron and TOC release during the EFCCM treatment of a 0.050 M Na_2SO_4 solution without pollutant at 2 mL min^{-1}. As depicted in Fig. S7, a minimal decomposition of NH_2-MIL-88B(Fe) occurred at natural pH ~6.2, yielding 1.8 mg L^{-1} iron and 6.7 mg L^{-1} TOC at long time (300 min). Note that only around 0.6 mg L^{-1} iron and 3.4 mg L^{-1} TOC were accumulated at 60 min (i.e., the time needed to destroy 85% NPX, Fig. 4c). In both scenarios, the final iron concentration was below the environmental standard (2 mg L^{-1}) [22]. The released TOC was originated from the organic ligands, which possess low toxicity but may contribute to total TOC and scavenge some $^{\bullet}OH$. In conclusion, the stability of the NH_2-MIL-88B(Fe)@CM for water treatment at near-neutral pH was high.

Undoubtedly, the reusability of the CM is one of the major aspects to be addressed for practical application. In Fig. 5a, its high reusability during the optimum EFCCM treatment of NPX solution after five consecutive cycles (90 min each) is demonstrated, considering that the CCM developed in this work is a first proof of concept. The NH_2-MIL-88B(Fe)@CM still maintained a high catalytic activity, with a removal efficiency of 86%, after the 5^{th} cycle. The slight loss of performance could be ascribed to both, deactivation and exfoliation of some of NH_2-MIL-88B(Fe) particles, as inferred from Fig. 5b. The first trial yielded the highest catalyst loss (12.5 mg), whereupon the value was kept very low during the subsequent trials. Indeed, the interaction between the top NH_2-MIL-88B(Fe) layer and the other layers on the CM surface was not able to stabilize all the catalyst particles, being partly lost during the first usage. However, the lack of catalyst stability that caused its partial exfoliation (i.e., mass loss) in the

1st run was not directly correlated with the largest performance decrease (Fig. 5a), which means that the interplay between catalyst loss (with alteration of pore exposure) and catalyst deactivation (i.e., alteration of the active site exposure) actually accounted for the loss of performance. Nevertheless, such mass loss did not impair the degradation performance so significantly.

3.5. NPX concentration decay and antifouling performance in urban wastewater

The ability of EFCCM to treat 0.060 mM NPX solutions in conditioned urban wastewater at pH 6.5 was further evaluated. The drug concentration decay presented in Fig. 6a informs about a smaller but progressive degradation in wastewater, attaining 82% removal at 90 min instead of 97% in Na_2SO_4. The presence of other pollutants and natural organic matter in wastewater, which may block membrane pores, occupy adsorption sites and consume •OH, limited the NPX destruction [44,52], although EFCCM was still highly effective.

The antifouling characteristics of the membranes are crucial for their scale-up. Fig. 6b shows the TMP change during: (i) The EFCCM treatment of NPX spiked into wastewater for 90 min (Fig. 6a), and (ii) the subsequent cleaning procedures. The TMP gradually increased from around 4.5 to 25.0 kPa during the NPX treatment, which is in contrast to the stable TMP recorded in 0.050 M Na_2SO_4 solution (Fig. 4b). This confirms that the presence of organic matter and other components in urban wastewater could promote the membrane fouling. Despite this, the NPX removal was still significant (Fig. 6a). In addition, an excellent cleaning methodology was devised by combining hot water backwash with EF self-cleaning. The TMP was almost halved upon hot water backwash, owing to the elimination of fouling agents found

on the CM. Nonetheless, these foulants were not completely removed, as deduced from the notably lower NPX concentration decay (i.e., 50%) attained at 90 min (Fig. S8). The residual impurities that adhered tightly to the membrane inner pores were subsequently removed via EF process, resulting in a complete and stable TMP recovery (Fig. 6b) and the obtention of a degradation profile analogous to the initial one (Fig. S8) [53]. The robust antifouling procedure allows the long-term use of the membrane in EFCCM.

3.6. Degradation routes of NPX and proposed reaction mechanism for the EFCCM process

As summarized in Table S1, seven main products were identified from NPX degradation by GC-MS, allowing the proposal of the degradation routes that appear in Fig. 7. The initial decarboxylation of the side chain of NPX (**1**), without or with •OH incorporation to the structure yielded compounds **2** and **3**, respectively. The latter was oxidized to form a ketone (compound **4**), which might arise directly from the oxidation of **1** as well. The synchronous oxidation of the same side chain of compounds **2** and **4** further led to the generation of compound **5**. Note that hydroxylation has been reported as the preferred degradation pathway in AOPs [54,55]. On the other hand, the production of compound **6** was achieved upon hydroxylation and demethylation of compound **4**, which is consistent with results reported for conventional EF treatment of NPX [56,57]. Finally, the sequential degradation of the naphthalene derivatives with partial or total cleavage of the rings yielded the aromatic and aliphatic compounds **7** and **8**. Note that Fig. 7 illustrates the first stages of the degradation, since successive ring-opening reactions are known to yield aliphatic compounds like short-chain carboxylic acids [1].

To ascertain the reaction mechanism for EFCCM process, the dominant reactive oxygen species generated was analyzed by EPR. As depicted in Fig. S9, the EPR spectrum exhibits the four typical intense peaks (intensity ratio of 1:2:2:1) of the DMPO-•OH adduct, corroborating the primary role of •OH.

Based on the findings discussed in this work, the mechanism for radical generation and NPX removal in EFCCM process is proposed in Fig. 8. H_2O_2 produced at the GDE surface through reaction (2) and NPX molecules were pumped toward the membrane surface and inner pores. NPX was then adsorbed onto hydrophilic and positively charged NH_2-MIL-88B(Fe) particles, whereas H_2O_2 was also easily adsorbed and its decomposition was catalyzed by the iron active sites to produce a large amount of •OH. The high concentration of NPX and •OH confined within the porous NH_2-MIL-88B(Fe) layers and membrane pores enabled their high reactivity, which led to the efficient NPX decay and retarded the membrane fouling. The outstanding redox cyclability of iron species in NH_2-MIL-88B(Fe) became crucial for the excellent •OH production. Overall, the NH_2-MIL-88B(Fe)@CM-assisted EF process shows several advantages over the single counterparts: (i) The NH_2-MIL-88B(Fe) coating on the CM increases the rejection of low molecular weight organic compounds; (ii) membrane filtration concentrates the organic molecules, offering greater accessibility to •OH and diminishing the destruction of these radicals in parasitic reactions; (iii) the uniform distribution of the catalyst on the membrane simplifies its recovery after the treatment thanks to a robust cleaning methodology.

4. Conclusions

A new type of CCM was successfully developed to integrate filtration and HEF processes for the efficient abatement of low molecular weight micropollutants in wastewater. Highly crystalline NH_2-MIL-88B(Fe) hexagonal micro-spindles were uniformly and firmly distributed on the CM or embedded in the micropores. The as-prepared NH_2-MIL-88B(Fe)@CM showed great mechanical strength, excellent hydrophilicity and enhanced rejection performance towards organics. This allowed that NPX, its byproducts and oxidant species became confined and concentrated in the tortuous pathways of the membrane. The successful coupling between membrane filtration and catalytic oxidation allowed a fast drug decay. The key parameters in EFCCM process were investigated, to conclude that the EFCCM is viable in a wide pH range and TMP is stable at relatively low flow rates. Under optimum EFCCM conditions, the decorated membrane partly lost its performance due to catalyst exfoliation combined with deactivation, although 86% NPX removal could be still obtained after five runs. Since the largest loss of performance was not directly correlated to initial catalyst loss, it is clear that the future improvement of the CCM activity should mainly rely on reactivation by rinsing to remove the adsorbed reaction byproducts. The great potential of the EFCCM process was further confirmed from the substantial NPX decay in urban wastewater. A simple strategy combining hot water backwash with EF mitigated the membrane fouling in that water matrix. Worth noticing, the feasibility to operate the optimized EFCCM process in continuous mode was also demonstrated, as the NPX concentration at the membrane outlet was reduced down to 1.5 mg L^{-1} or less from the beginning of the electrolysis.

Acknowledgements

The authors kindly acknowledge the financial support from the Research Grants Council (RGC) of the Hong Kong SAR Government (17210219 and T21-711/16-R), the Fundamental Research Funds for the Central Universities, China (No. 02190052020062), as well as from project PID2019-109291RB-I00 (MCIN/AEI/ 10.13039/501100011033, Spain).

References

[1] E. Brillas, I. Sirés, M.A. Oturan, Electro-Fenton process and related electrochemical technologies based on Fenton's reaction chemistry, Chem. Rev. 109 (2009) 6570-6631.

[2] X. Du, M.A. Oturan, M. Zhou, N. Belkessa, P. Su, J. Cai, C. Trellu, E. Mousset, Nanostructured electrodes for electrocatalytic advanced oxidation processes: From materials preparation to mechanisms understanding and wastewater treatment applications, Appl. Catal. B: Environ. 296 (2021) 120332.

[3] I. Sirés, E. Brillas, Upgrading and expanding the electro-Fenton and related processes, Curr. Opin. Electrochem. 27 (2021) 100686.

[4] V. Melin, P. Salgado, A. Thiam, A. Henríquez, H.D. Mansilla, J. Yáñez, C. Salazar, Study of degradation of amitriptyline antidepressant by different electrochemical advanced oxidation processes, Chemosphere 274 (2021) 129683.

[5] M.F. Murrieta, J.L. Nava, Electrosynthesis of hypochlorous acid in a filter-press electrolyzer and its modeling in dilute chloride solutions, J. Electroanal. Chem. 892 (2021) 115286.

[6] Z. Ye, D.R.V. Guelfi, G. Alvarez, F. Alcaide, E. Brillas, I. Sirés, Enhanced electrocatalytic production of H_2O_2 at Co-based air-diffusion cathodes for the photoelectro-Fenton treatment of bronopol, Appl. Catal. B: Environ. 247 (2019) 191-199.

[7] Q. Zhang, M. Zhou, G. Ren, Y. Li, Y. Li, X. Du, Highly efficient electrosynthesis of hydrogen peroxide on a superhydrophobic three-phase interface by natural air diffusion, Nature Commun. 11 (2020) 1731.

[8] Y. Zhang, G. Daniel, S. Lanzalaco, A.A. Isse, A. Facchin, A. Wang, E. Brillas, C. Durante, I. Sirés, H_2O_2 production at gas-diffusion cathodes made from agarose-derived carbons with different textural properties for acebutolol degradation in chloride media, J. Hazard. Mater. 423 (2022) 127005.

[9] H. Lin, N. Oturan, J. Wu, H. Zhang, M.A. Oturan, Cold incineration of sucralose in aqueous solution by electro-Fenton process, Sep. Purif. Technol. 173 (2017) 218-225.

[10] P. Cao, X. Quan, K. Zhao, S. Chen, H. Yu, J. Niu, Selective electrochemical H_2O_2 generation and activation on a bifunctional catalyst for heterogeneous electro-Fenton catalysis, J. Hazard Mater. 382 (2020) 121102.

[11] G. Daniel, Y. Zhang, S. Lanzalaco, F. Brombin, T. Kosmala, G. Granozzi, A. Wang, E. Brillas, I. Sirés, C. Durante, Chitosan-derived nitrogen-doped carbon electrocatalyst for a sustainable upgrade of oxygen reduction to hydrogen peroxide in UV-assisted electro-Fenton water treatment, ACS Sustain. Chem. Eng. 8 (2020) 14425-14440.

[12] H. Li, X.Y. Ji, X.Q. Pan, C. Liu, W.J. Liu, Ionothermal carbonization of biomass to construct Fe, N-doped biochar with prominent activity and recyclability as cathodic

catalysts in heterogeneous electro-Fenton, ACS EST Engg. 1 (2021) 21-31.

[13] J.Y. Lu, Y.R. Yuan, X. Hu, W.J. Liu, C.X. Li, H.Q. Liu, W.W. Li, MOF-derived Fe_2O_3/Nitrogen/Carbon composite as a stable heterogeneous electro-Fenton catalyst, Ind. Eng. Chem. Res. 59 (2020) 1800-1808.

[14] Z. Ye, J.A. Padilla, E. Xuriguera, J.L. Beltran, F. Alcaide, E. Brillas, I. Sirés, A highly stable metal-organic framework-engineered FeS_2/C nanocatalyst for heterogeneous electro-Fenton treatment: validation in wastewater at mild pH, Environ. Sci. Technol. 54 (2020) 4664-4674.

[15] C. Lai, X. Shi, L. Li, M. Cheng, X. Liu, S. Liu, B. Li, H. Yi, L. Qin, M. Zhang, N. An, Enhancing iron redox cycling for promoting heterogeneous Fenton performance: A review, Sci. Total Environ. 775 (2021) 145850.

[16] T. Yang, D. Yu, D. Wang, T. Yang, Z. Li, M. Wu, M. Petru, J. Crittenden, Accelerating Fe(III)/Fe(II) cycle *via* Fe(II) substitution for enhancing Fenton-like performance of Fe-MOFs, Appl. Catal. B: Environ. 286 (2021) 119859.

[17] M. Cheng, C. Lai, Y. Liu, G. Zeng, D. Huang, C. Zhang, L. Qin, L. Hu, C. Zhou, W. Xiong, Metal-organic frameworks for highly efficient heterogeneous Fenton-like catalysis, Coord. Chem. Rev. 368 (2018) 80-92.

[18] Y. He, Z. Wang, H. Wang, Z. Wang, G. Zeng, P. Xu, D. Huang, M. Chen, B. Song, H. Qin, Y. Zhao, Metal-organic framework-derived nanomaterials in environment related fields: fundamentals, properties and applications, Coord. Chem. Rev. 429 (2021) 213618.

[19] S. Lu, L. Liu, H. Demissie, G. An, D. Wang, Design and application of metal-organic

frameworks and derivatives as heterogeneous Fenton-like catalysts for organic wastewater treatment: A review, Environ. Int. 146 (2021) 106273.

[20] N. Thomas, D.D. Dionysiou, S.C. Pillai, Heterogeneous Fenton catalysts: A review of recent advances, J. Hazard. Mater. 404 (2021) 124082.

[21] M. Ma, H. Noei, B. Mienert, J. Niesel, E. Bill, M. Muhler, R.A. Fischer, Y. Wang, U. Schatzschneider, N. Metzler-Nolte, Iron metal-organic frameworks MIL-88B and NH_2-MIL-88B for the loading and delivery of the gasotransmitter carbon monoxide, Chem. A Eur. J. 19 (2013) 6785-6790.

[22] M. Ahmad, X. Quan, S. Chen, H. Yu, Tuning Lewis acidity of MIL-88B-Fe with mix-valence coordinatively unsaturated iron centers on ultrathin Ti_3C_2 nanosheets for efficient photo-Fenton reaction, Appl. Catal. B: Environ (2020) 264, 118534.

[23] C. Gao, S. Chen, X. Quan, H. Yu, Y. Zhang, Enhanced Fenton-like catalysis by iron-based metal organic frameworks for degradation of organic pollutants, J. Catal. 356 (2017) 125-132.

[24] C. Gao, Y. Su, X. Quan, V.K. Sharma, S. Chen, H. Yu, Y. Zhang, J. Niu, Electronic modulation of iron-bearing heterogeneous catalysts to accelerate Fe(III)/Fe(II) redox cycle for highly efficient Fenton-like catalysis, Appl. Catal. B: Environ. 276 (2020) 119016.

[25] T. Van Tran, V.H. Nguyen, L.X. Nong, H.T.T. Nguyen, D.T.C. Nguyen, T.T. Nguyen, H.T.T. Nguyen, T.D. Nguyen, Hexagonal Fe-based MIL-88B nanocrystals with NH_2 functional groups accelerating oxytetracycline capture via hydrogen bonding, Surf. Interfaces 20 (2020) 100605.

[26] F. Liu, H. Yao, S. Sun, W. Tao, T. Wei, P. Sun, Photo-Fenton activation mechanism and antifouling performance of an FeOCl-coated ceramic membrane, Chem. Eng. J. 402 (2020) 125477.

[27] K.V. Plakas, A. Mantza, S.D. Sklari, V.T. Zaspalis, A.J. Karabelas, Heterogeneous Fenton-like oxidation of pharmaceutical diclofenac by a catalytic iron-oxide ceramic microfiltration membrane, Chem. Eng. J. 373 (2019) 700-708.

[28] A. Urtiaga, Electrochemical technologies combined with membrane filtration, Curr. Opin. Electrochem. 27 (2021) 100691.

[29] P. Kumari, N. Bahadur, L.F. Dumée, Photo-catalytic membrane reactors for the remediation of persistent organic pollutants – A review, Sep. Purif. Technol. 230 (2020) 115878.

[30] S. Sun, H. Yao, W. Fu, L. Hua, G. Zhang, W. Zhang, Reactive photo-Fenton ceramic membranes: Synthesis, characterization and antifouling performance, Water Res. 144 (2018) 690-698.

[31] S. Sun, H. Yao, W. Fu, S. Xue, W. Zhang, Enhanced degradation of antibiotics by photo-Fenton reactive membrane filtration, J. Hazard. Mater. 386 (2020) 121955.

[32] H. Huang, K. Schwab, J.G. Jacangelo, Pretreatment for low pressure membranes in water treatment: A review, Environ. Sci. Technol. 43 (2009) 3011-3019.

[33] J. Zheng, Z. Wang, J. Ma, S. Xu, Z. Wu, Development of an electrochemical ceramic membrane filtration system for efficient contaminant removal from waters, Environ. Sci. Technol. 52 (2018) 4117-4126.

[34] C. Li, W. Sun, Z. Lu, X. Ao, S. Li, Ceramic nanocomposite membranes and membrane

fouling: A review, Water Res. 175 (2020) 115647.

[35] H. Wu, X. Xu, L. Shi, Y. Yin, L. Zhang, Z. Wu, X. Duan, S. Wang, H. Sun, Manganese oxide integrated catalytic ceramic membrane for degradation of organic pollutants using sulfate radicals, Water Res. 167 (2019) 115110.

[36] K. Changanaqui, H. Alarcón, E. Brillas, I. Sirés, Blue LED light-driven photoelectrocatalytic removal of naproxen from water: Kinetics and primary by-products, J. Electroanal. Chem. 867 (2020) 114192.

[37] S. Luo, L. Gao, Z. Wei, R. Spinney, D.D. Dionysiou, W.-P. Hu, L. Chai, R. Xiao, Kinetic and mechanistic aspects of hydroxyl radical–mediated degradation of naproxen and reaction intermediates, Water Res. 137 (2018) 233-241.

[38] L. Xu, X. Ma, J. Niu, J. Chen, C. Zhou, Removal of trace naproxen from aqueous solution using a laboratory-scale reactive flow-through membrane electrode, J. Hazard. Mater. 379 (2019) 120692.

[39] Z. Ye, G.E.M. Schukraft, A. L'Hermitte, Y. Xiong, E. Brillas, C. Petit, I. Sirés, Mechanism and stability of an Fe-based 2D MOF during the photoelectro-Fenton treatment of organic micropollutants under UVA and visible light irradiation, Water Res. 184 (2020) 115986.

[40] L. Shao, Z. Yu, X. Li, X. Li, H. Zeng, X. Feng, Carbon nanodots anchored onto the metal-organic framework NH_2-MIL-88B(Fe) as a novel visible light-driven photocatalyst: photocatalytic performance and mechanism investigation, Appl. Surf. Sci. 505 (2020) 144616.

[41] X. Yi, X. He, F. Yin, T. Yang, B. Chen, G. Li, NH_2-MIL-88B-Fe for electrocatalytic N_2

fixation to NH_3 with high Faradaic efficiency under ambient conditions in neutral electrolyte, J. Mater. Sci. 55 (2020) 12041-12052.

[42] J. Long, S. Wang, Z. Ding, S. Wang, Y. Zhou, L. Huang, X. Wang, Amine-functionalized zirconium metal-organic framework as efficient visible-light photocatalyst for aerobic organic transformations, Chem. Commun. 48 (2012) 11656-11658.

[43] R. Yuan, C. Yue, J. Qiu, F. Liu, A. Li, Highly efficient sunlight-driven reduction of Cr(VI) by TiO_2@NH_2-MIL-88B(Fe) heterostructures under neutral conditions, Appl. Catal. B: Environ. 251 (2019) 229-239.

[44] Z. Ye, J.A. Padilla, E. Xuriguera, E. Brillas, I. Sirés, Magnetic MIL(Fe)-type MOF-derived N-doped nano-ZVI@C rods as heterogeneous catalyst for the electro-Fenton degradation of gemfibrozil in a complex aqueous matrix, Appl. Catal. B: Environ. 266 (2020) 118604.

[45] D. Wang, F. Jia, H. Wang, F. Chen, Y. Fang, W. Dong, G. Zeng, X. Li, Q. Yang, X. Yuan, Simultaneously efficient adsorption and photocatalytic degradation of tetracycline by Fe-based MOFs, J. Colloid Interface Sci. 519 (2018) 273-284.

[46] N. Wang, T. Liu, H. Shen, S. Ji, J.R. Li, R. Zhang, Ceramic tubular MOF hybrid membrane fabricated through in situ layer-by-layer self-assembly for nanofiltration, AIChE J. 62 (2016) 538-546.

[47] Y. Fan, Y. Zhou, Y. Feng, P. Wang, X. Li, K. Shih, Fabrication of reactive flat-sheet ceramic membranes for oxidative degradation of ofloxacin by peroxymonosulfate, J. Membr. Sci. 611 (2020) 118302.

[48] W.L. Sun, H.B. Li, H.M. Li, S. Li, X.Q. Cao, Adsorption mechanisms of ibuprofen and

naproxen to UiO-66 and UiO-66-NH_2: Batch experiment and DFT calculation, Chem. Eng. J. 360 (2019) 645-653.

[49] J. Benito, M. Fenero, S. Sorribas, B. Zornoza, K.J. Msayib, N.B. McKeown, C. Téllez, J. Coronas, I. Gascón, Fabrication of ultrathin films containing the metal organic framework Fe-MIL-88B-NH_2 by the Langmuir-Blodgett technique, Colloids Surf. Physicochem. Eng. Aspects 470 (2015) 161-170.

[50] H. Lin, Q. Fang, W. Wang, G. Li, J. Guan, Y. Shen, J. Ye, F. Liu, Prussian blue/PVDF catalytic membrane with exceptional and stable Fenton oxidation performance for organic pollutants removal, Appl. Catal. B: Environ. 273 (2020) 119047.

[51] S. Lanzalaco, I. Sirés, M.A. Sabatino, C. Dispenza, O. Scialdone, A. Galia, Synthesis of polymer nanogels by electro-Fenton process: investigation of the effect of main operation parameters, Electrochim. Acta 246 (2017) 812-822.

[52] Y. Bao, W.J. Lee, T.-T. Lim, R. Wang, X. Hu, Pore-functionalized ceramic membrane with isotropically impregnated cobalt oxide for sulfamethoxazole degradation and membrane fouling elimination: synergistic effect between catalytic oxidation and membrane separation, Appl. Catal. B: Environ. 254 (2019) 37-46.

[53] X. Wang, M. Sun, Y. Zhao, C. Wang, W. Ma, M.S. Wong, M. Elimelech, In situ electrochemical generation of reactive chlorine species for efficient ultrafiltration membrane self-cleaning, Environ. Sci. Technol. 54 (2020) 6997-7007.

[54] A. Ghauch, A.M. Tuqan, N. Kibbi, Naproxen abatement by thermally activated persulfate in aqueous systems, Chem. Eng. J. 279 (2015) 861-873.

[55] F. Wang, Y. Wang, Y. Feng, Y. Zeng, Z. Xie, Q. Zhang, Y. Su, P. Chen, Y. Liu, K. Yao, W. Lv, G. Liu, Novel ternary photocatalyst of single atom-dispersed silver and carbon quantum dots co-loaded with ultrathin g-C_3N_4 for broad spectrum photocatalytic degradation of naproxen, Appl. Catal. B: Environ. 221 (2018) 510-520.

[56] G. Coria, I. Sirés, E. Brillas, J.L. Nava, Influence of the anode material on the degradation of naproxen by Fenton-based electrochemical processes, Chem. Eng. J. 304 (2016) 817-825.

[57] H. Mohammadi, B. Bina, A. Ebrahimi, A novel three-dimensional electro-Fenton system and its application for degradation of anti-inflammatory pharmaceuticals: modeling and degradation pathways, Process Saf. Environ. 117 (2018) 200-213.

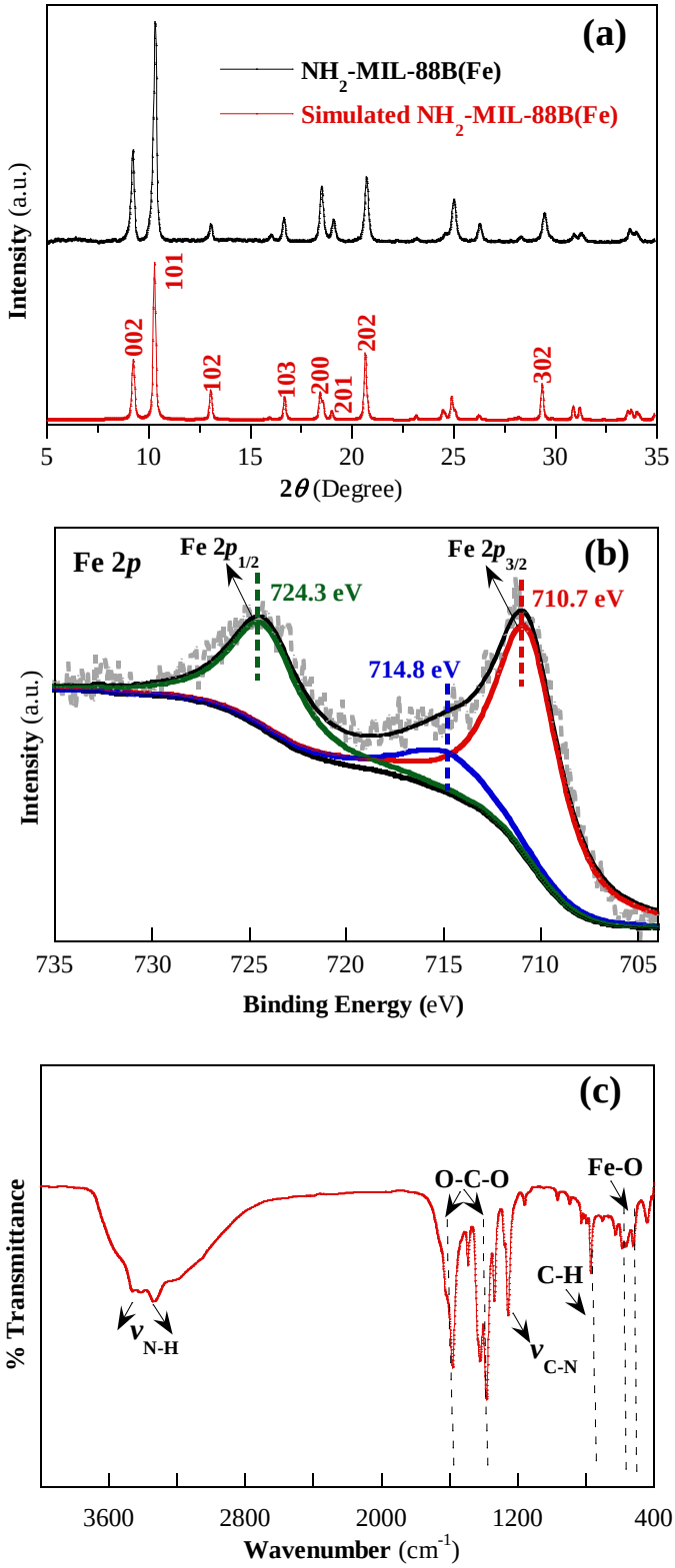

Fig. 1. Physicochemical characterization of the as-prepared NH_2-MIL-88B(Fe): (a) XRD pattern, (b) Fe 2*p* XPS core-level spectrum and (c) FTIR spectrum.

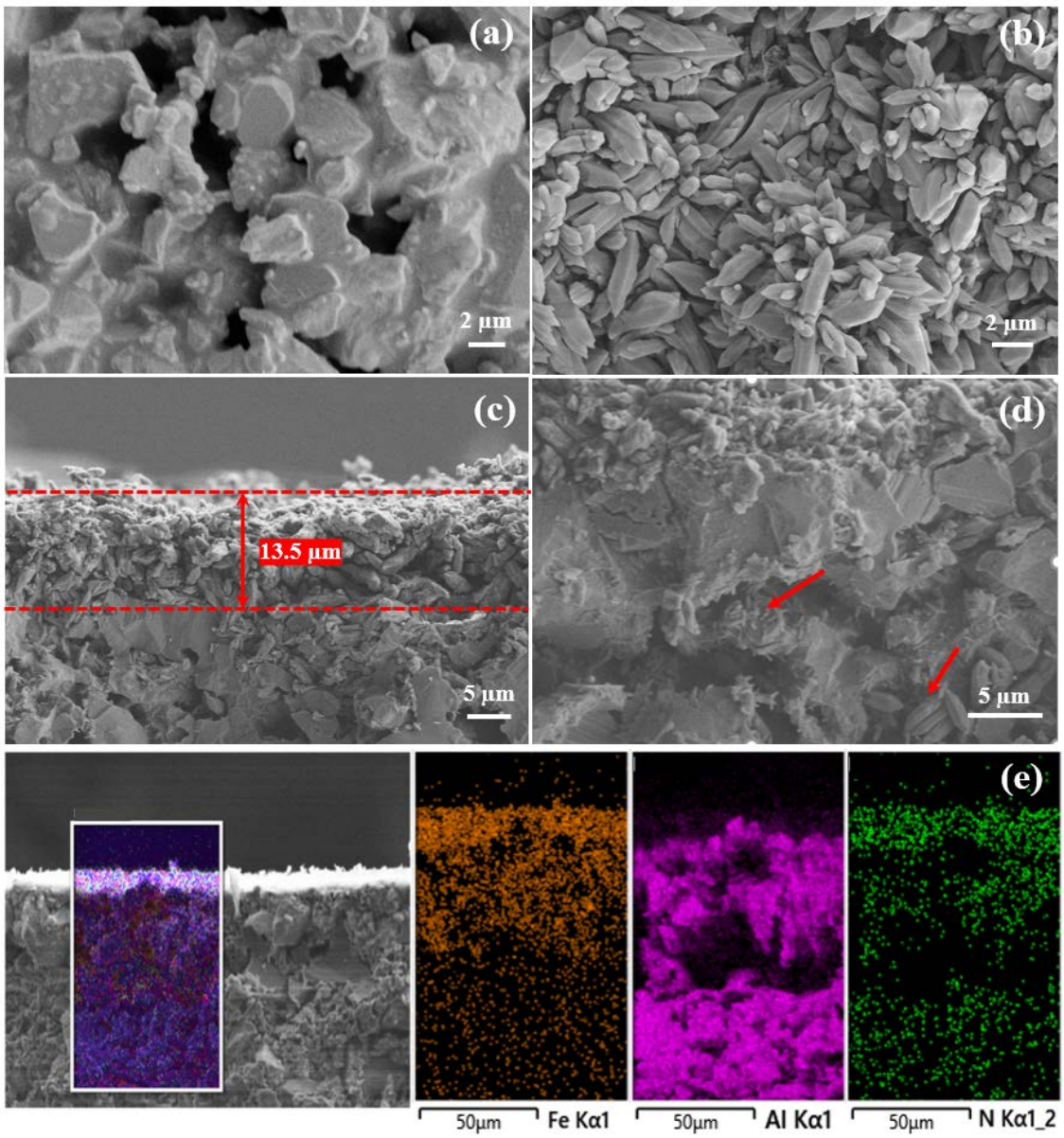

Fig. 2. SEM images of the (a) pristine ceramic membrane, (b-d) surface, cross-section and interior of the NH_2-MIL-88B(Fe)@CM, respectively, and (e) elemental mapping of the cross-section of the NH_2-MIL-88B(Fe)@CM.

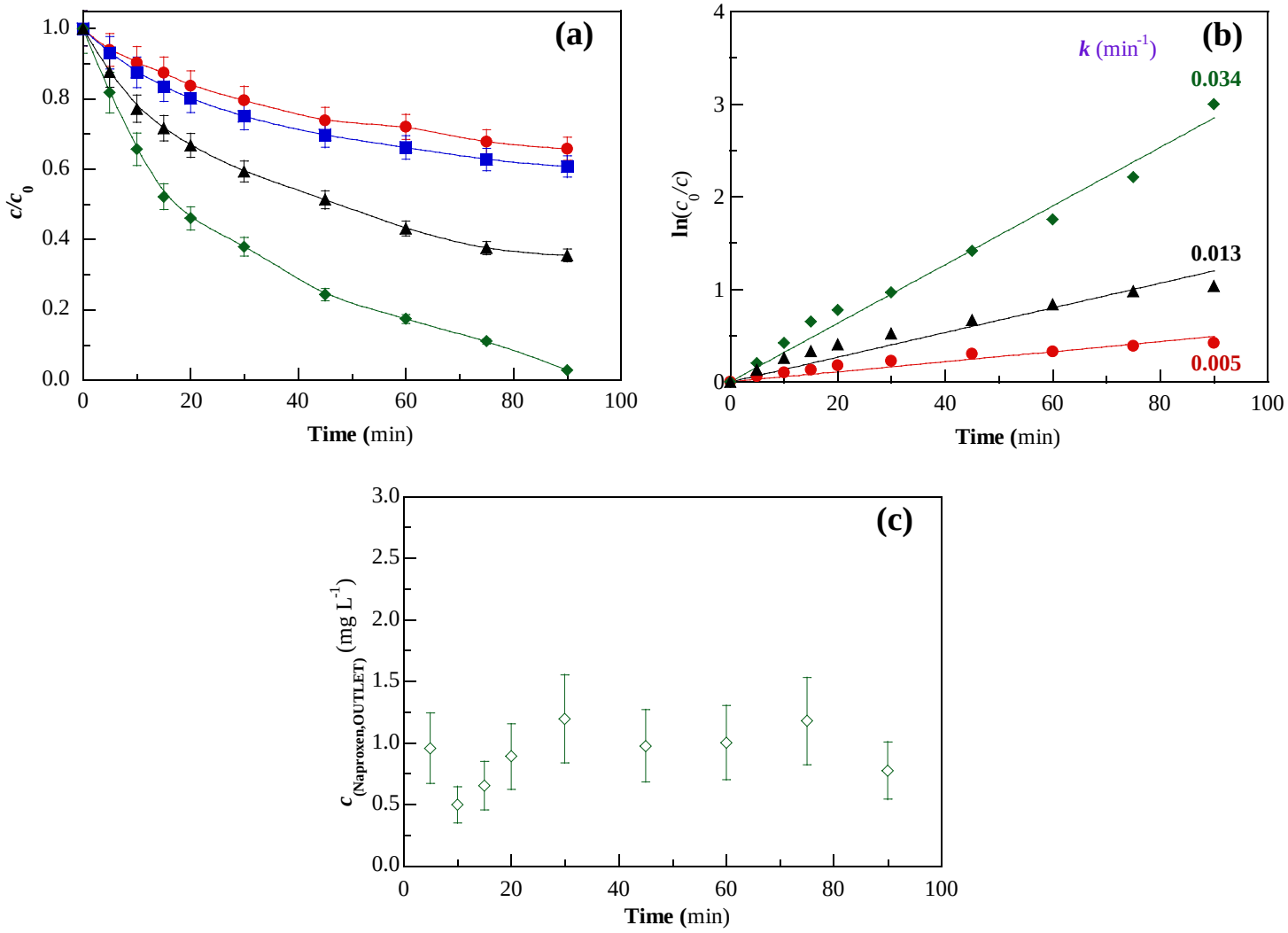

Fig. 3. (a) Normalized naproxen concentration decay during the treatment of 180 mL of 0.060 mM (10 mg C L^{-1}) naproxen sodium solutions containing 0.050 M Na_2SO_4 at natural pH ~6.2 by: (●) EO, (■) filtration with the NH_2-MIL-88B(Fe)@CM at flow rate of 2 mL min^{-1}, (▲) heterogeneous EF process catalyzed by NH_2-MIL-88B(Fe) supported on the surface of the ceramic membrane at flow rate of 0 mL min^{-1}, and (◆) integrated heterogeneous EF with catalytic ceramic membrane (EFCCM) process at flow rate of 2 mL min^{-1}. (b) Pseudo-first-order kinetic analysis of naproxen decays shown in plot (a); the resulting kinetic constants are included. (c) Naproxen concentration at the membrane outlet during the EFCCM treatment. In electrochemical assays, an IrO_2/air-diffusion cell was used at 50 mA and 25 ºC.

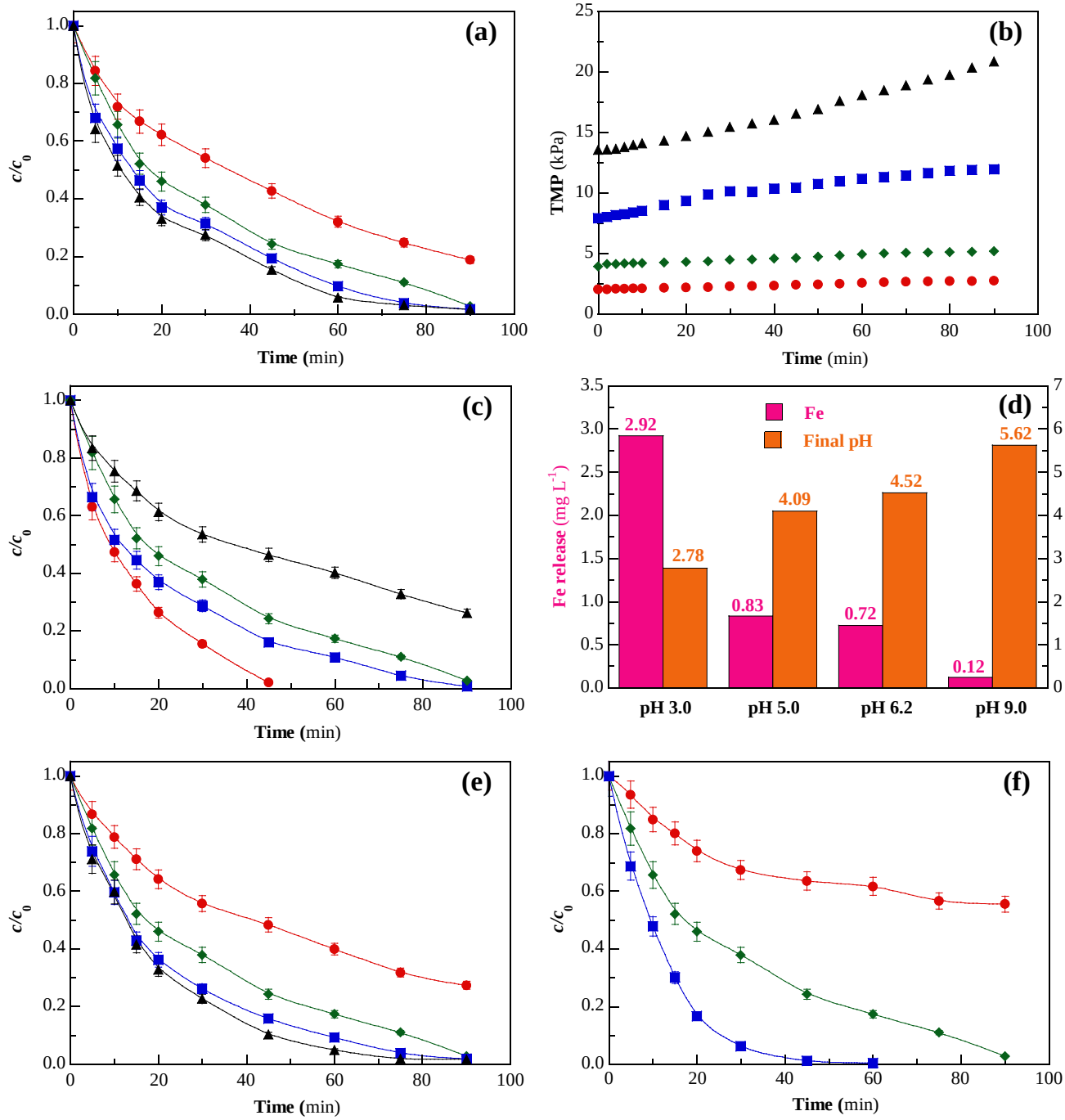

Fig. 4. (a, c, e, f) Normalized naproxen concentration decay during the EFCCM treatment of 180 mL of 0.060 mM drug solutions with 0.050 M Na_2SO_4 (except in plot f) using an IrO_2/air-diffusion cell. In plot a, effect of flow rate at pH 6.2 and 50 mA: (●) 1, (◆) 2, (■) 4 and (▲) 6 mL min^{-1}; in plot c, effect of initial pH at 2 mL min^{-1} and 50 mA: (●) 3.0, (■) 5.0, (◆) 6.2 and (▲) 9.0; in plot e, effect of applied current at pH 6.2 and 2 mL min^{-1}: (●) 25, (◆) 50, (■) 75 and (▲) 100 mA; in plot f, effect of the electrolyte composition at pH 6.2, 50 mA and 2 mL min^{-1}: (●) 0.041 M Na_2SO_4 + 0.009 M $NaHCO_3$ solution, (◆) 0.050 M Na_2SO_4 solution and (■) 0.025 M Na_2SO_4 + 0.035 M NaCl solution. (b) Increase in transmembrane pressure (TMP) during the trials described in plot a. (d) Final dissolved iron concentration and pH at the end of the trials described in plot c.

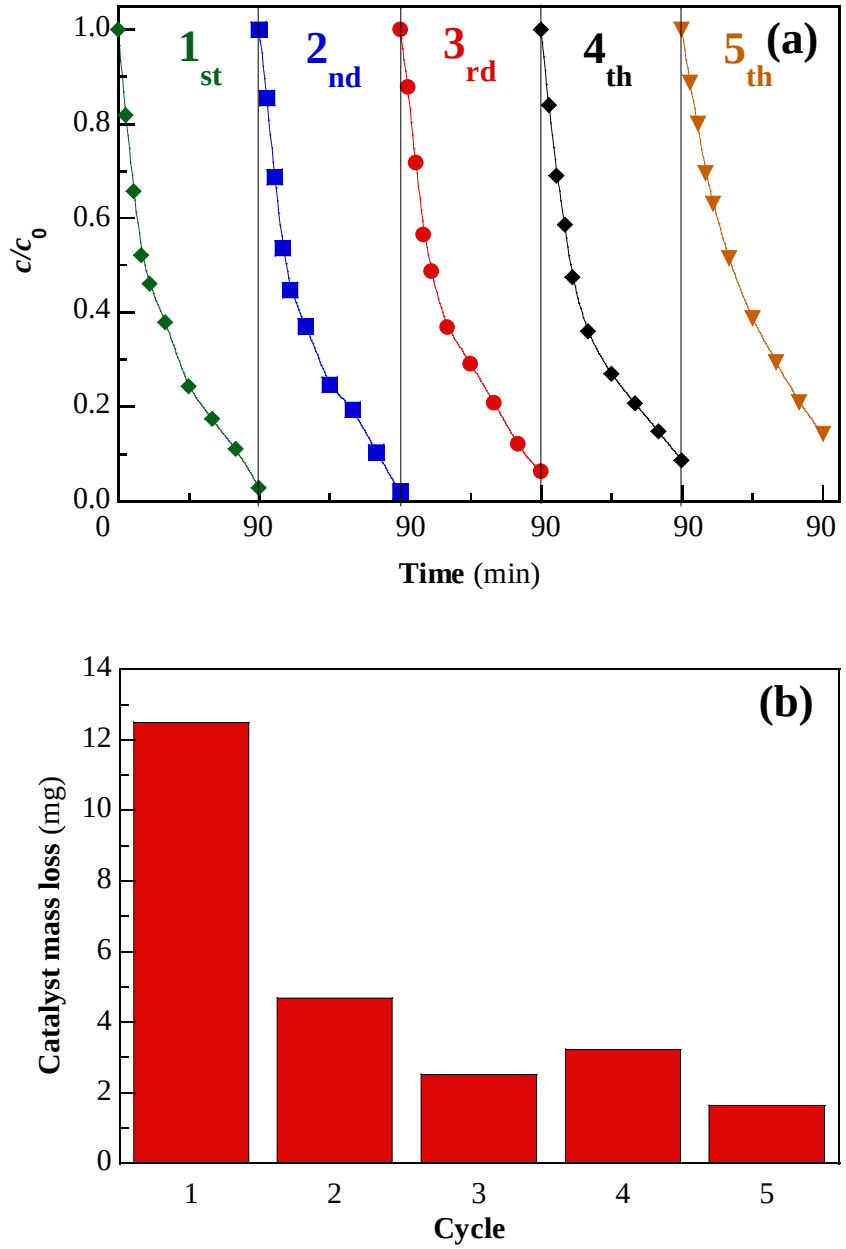

Fig. 5. (a) Time course of normalized naproxen concentration and (b) NH_2-MIL-88B(Fe) mass loss during the EFCCM treatment of naproxen solution with 0.050 M Na_2SO_4 (described in Fig. 3a) for five consecutive cycles (90 min each).

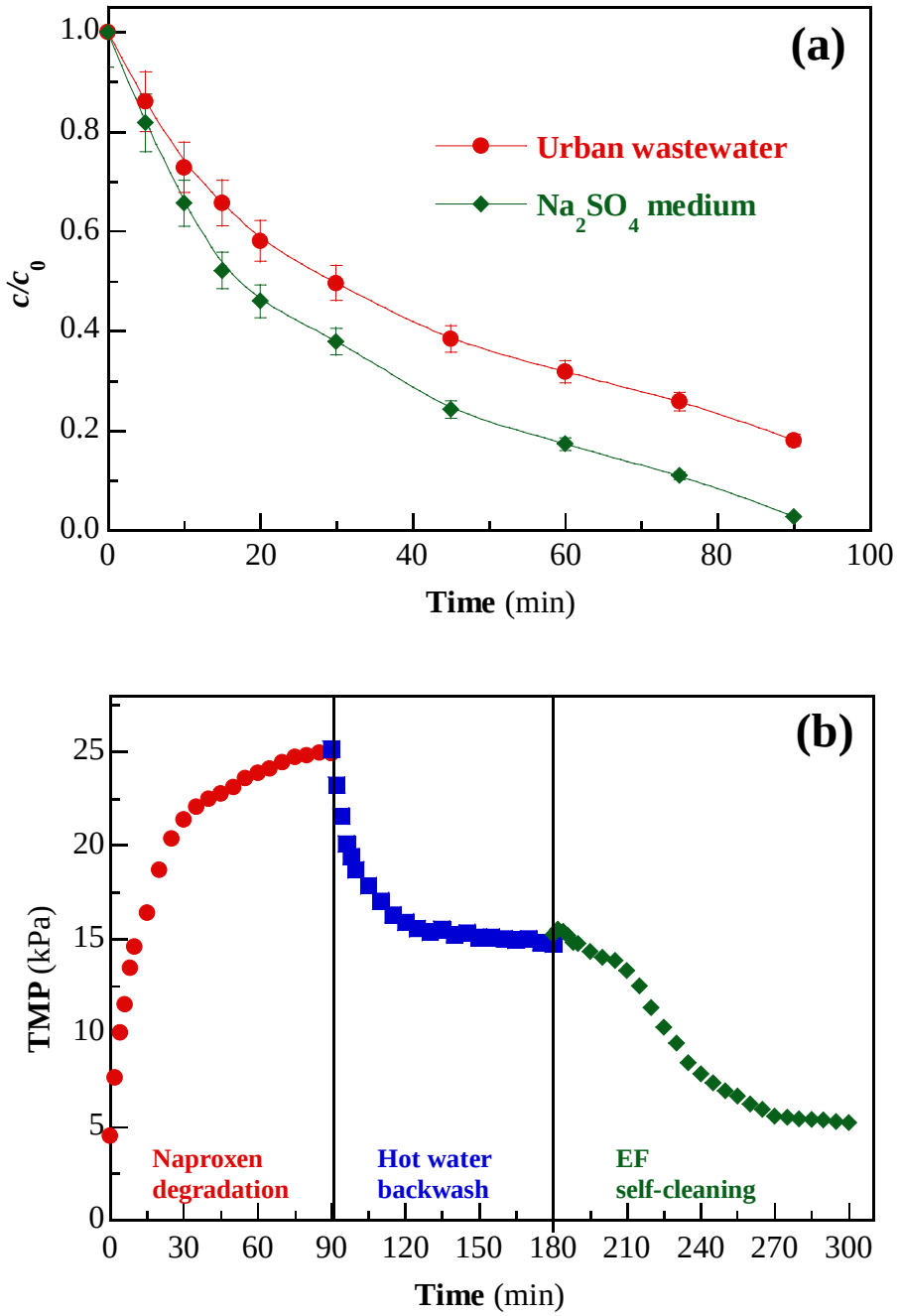

Fig. 6. Compared EFCCM treatment of naproxen solutions either in (◆) 0.050 M Na_2SO_4 or (●) urban wastewater under conditions described in Fig. 3a using the IrO_2/air-diffusion cell. (b) TMP variation during (●) naproxen degradation via EFCCM process in urban wastewater, and during subsequent membrane cleaning by (■) hot water backwash at 70 ºC and (◆) EF self-cleaning with 0.050 M Na_2SO_4 solution at 100 mA. The cleaning was always made at flow rate of 2 mL min^{-1}.

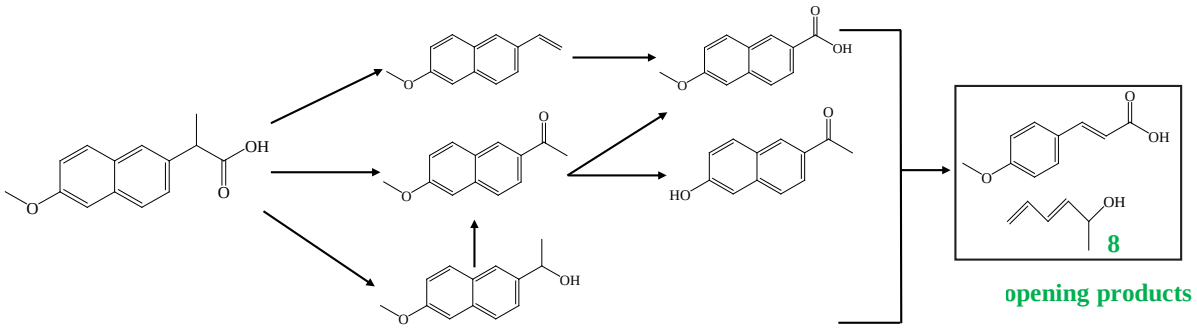

Fig. 7. First stages of the degradation pathway proposed for naproxen during the EFCCM treatment at natural pH.

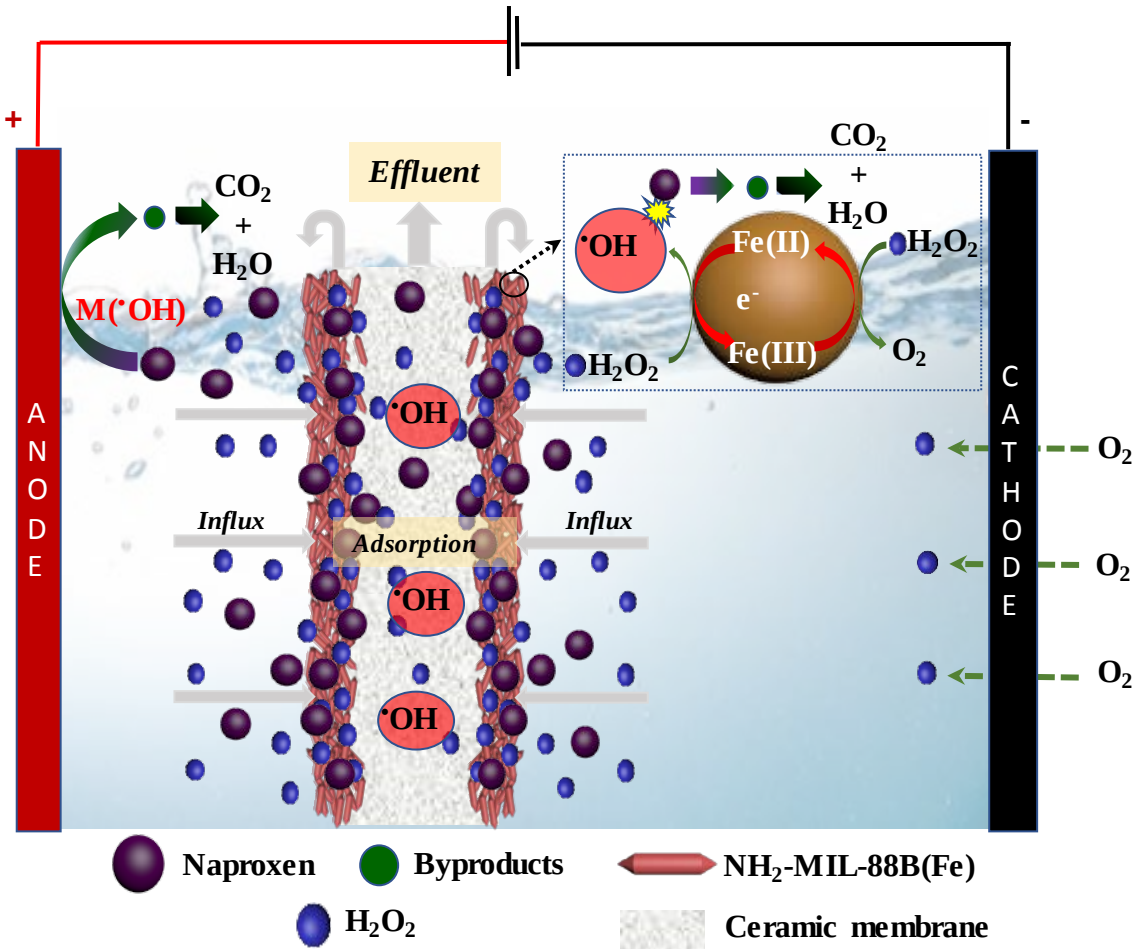

Fig. 8. Proposed mechanism for the integrated EFCCM process with the NH_2-MIL-88B(Fe)@CM at mild pH, with overall mineralization of byproducts.